Metformin promotes angiogenesis and functional recovery in aged mice after spinal cord injury by adenosine monophosphate-activated protein kinase/endothelial nitric oxide synthase pathway

Jin-Yun Zhao[1, 2, 3, 4], Xiao-Long Sheng[1, 2, 3, 4], Cheng-Jun Li[1, 2, 3, 4], Tian Qin[1, 2, 3, 4], Run-Dong He[1, 2, 3, 4], Guo-Yu Dai[1, 2, 3, 4], Yong Cao[1, 2, 3, 4], Hong-Bin Lu[2, 3, 4, 5], Chun-Yue Duan[1, 2, 3, 4, *], Jian-Zhong Hu[1, 2, 3, 4, *]

https://doi.org/10.4103/1673-5374.360245

Date of submission: March 31, 2022

Date of decision: July 22, 2022

Date of acceptance: September 17, 2022

Date of web publication: November 9, 2022

From the Contents

Graphical Abstract

Effects of metformin on angiogenesis and hindlimb motor recovery following spinal cord injury in the aged mice

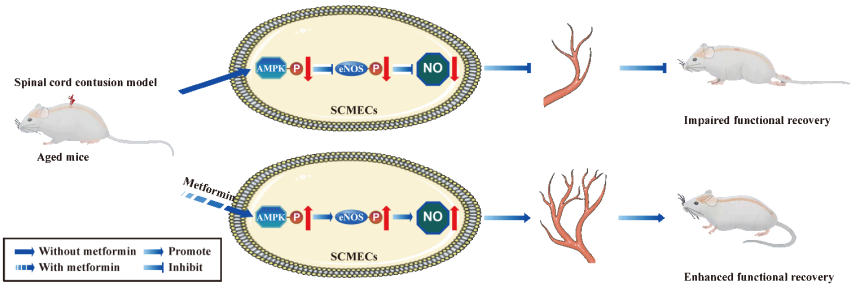

Abstract

Treatment with metformin can lead to the recovery of pleiotropic biological activities after spinal cord injury. However, its effect on spinal cord injury in aged mice remains unclear. Considering the essential role of angiogenesis during the regeneration process, we hypothesized that metformin activates the adenosine monophosphate-activated protein kinase/endothelial nitric oxide synthase pathway in endothelial cells, thereby promoting microvascular regeneration in aged mice after spinal cord injury. In this study, we established young and aged mouse models of contusive spinal cord injury using a modified Allen method. We found that aging hindered the recovery of neurological function and the formation of blood vessels in the spinal cord. Treatment with metformin promoted spinal cord microvascular endothelial cell migration and blood vessel formation *in vitro*. Furthermore, intraperitoneal injection of metformin in an *in vivo* model promoted endothelial cell proliferation and increased the density of new blood vessels in the spinal cord, thereby improving neurological function. The role of metformin was reversed by compound C, an adenosine monophosphate-activated protein kinase inhibitor, both *in vivo* and *in vitro*, suggesting that the adenosine monophosphate-activated protein kinase/endothelial nitric oxide synthase pathway likely regulates metformin-mediated angiogenesis after spinal cord injury. These findings suggest that metformin promotes vascular regeneration in the injured spinal cord by activating the adenosine monophosphate-activated protein kinase/endothelial nitric oxide synthase pathway, thereby improving the neurological function of aged mice after spinal cord injury.

Key Words: adenosine monophosphate-activated protein kinase/endothelial nitric oxide synthase pathway; angiogenesis; aged mice; compound C; metformin; spinal cord injury

Introduction

Traumatic spinal cord injury (SCI), when not fatal, frequently leads to permanent deficits in sensory and motor function. Despite major progress in neuro-therapeutic approaches for SCI, no clinically curative treatments are currently available. As the population ages, the social burden of older patients with SCI is rapidly growing (Devivo, 2012; Singh et al., 2014).

Recently there has been increasing interest in understanding the effects of aging on the pathological changes that occur after SCI. SCI is characterized by acute mechanical injury, causing the rupture of blood vessels, which triggers a cascade of secondary injuries (Graumann et al., 2011; Figley et al., 2014). After trauma, blood vessels undergo significant remodeling, which is vital for the survival of neuronal tissue (Sapieha, 2012; Ni et al., 2019). In addition, the structure of the microvasculature changes dramatically due to the induction of angiogenesis (Ng et al., 2011; Figley et al., 2014). New blood vessels grow into the lesion site to deliver nutrients that promote SCI repair (Figley et al., 2014). However, the effect of aging on vessel regeneration after SCI remains unclear.

The biguanide metformin has been used to treat type 2 diabetes and metabolic syndrome since the 1960s. More recently, increasing evidence has shown that metformin has important effects on cancer (Xu et al., 2015a) and polycystic ovary syndrome (Tao et al., 2018; Ali et al., 2019). Metformin is also cardioprotective (Calvert et al., 2008), suggesting that metformin-based therapy could be used to treat age-related diseases. In fact, studies have shown that metformin can delay the aging process (Barzilai et al., 2016; Piskovatska et al., 2020; Alhowail and Chigurupati, 2022), reduce aging-related inflammation (Bharath et al., 2020), and positively modulate the gut (Pollak,

[1]Department of Spine Surgery and Orthopedics, Xiangya Hospital, Central South University, Changsha, Hunan Province, China; [2]Key Laboratory of Organ Injury, Aging and Regenerative Medicine of Hunan Province, Changsha, Hunan Province, China; [3]National Clinical Research Center for Geriatric Disorders, Xiangya Hospital, Central South University, Changsha, Hunan Province, China; [4]Hunan Engineering Research Center of Sports and Health, Changsha, Hunan Province, China; [5]Department of Sports Medicine, Research Centre of Sports Medicine, Xiangya Hospital, Central South University, Changsha, Hunan Province, China

***Correspondence to:** Jian-Zhong Hu, PhD, jianzhonghu@hotmail.com; Chun-Yue Duan, PhD, docdcy@qq.com.
https://orcid.org/0000-0002-6874-4853 (Chun-Yue Duan)

Funding: *This work was supported by the Natural Nature Science Foundation of China, Nos. 82030071, 81874004; and the Science and Technology Major Project of Changsha, No. kh2103008 (all to JZH).*

How to cite this article: *Zhao JY, Sheng XL, Li CJ, Qin T, He RD, Dai GY, Cao Y, Lu HB, Duan CY, Hu JZ (2023) Metformin promotes angiogenesis and functional recovery in aged mice after spinal cord injury by adenosine monophosphate-activated protein kinase/endothelial nitric oxide synthase pathway. Neural Regen Res 18(7):1553-1562.*

2017). In addition, it has extensive effects in the central nervous system, showing benefit in the treatment of conditions such as Parkinson's disease (Paudel et al., 2020), Huntington's disease (Vázquez-Manrique et al., 2016), epilepsy (Sanz et al., 2021), and cerebral ischemia/reperfusion injury (Leech et al., 2019). Metformin is thought to modulate autophagy, inflammation, and neuronal apoptosis in the context of SCI in young rodent animals, which could help improve functional recovery (Wang et al., 2016; Zhang et al., 2017b; Song et al., 2021). Furthermore, metformin treatment not only ameliorates oxidative stress and stabilizes microtubules (Wang et al., 2020), but also prevents blood-spinal cord barrier breakdown by reducing the production of matrix metalloproteinase-9 and the amount of infiltrating neutrophils (Zhang et al., 2017a), reinforcing its potential therapeutic benefits in adult female SCI rats. However, it remains unclear whether metformin administration promotes robust vascular regeneration, thereby conferring neuroprotective effects and promoting functional recovery, especially in aged mice post-SCI, and what mechanisms may underlie these effects.

The present work focused on investigating whether angiogenesis is attenuated in aged mice after SCI. The results show that metformin affects blood vessel formation both *in vitro* and *in vivo* through the adenosine monophosphate-activated protein kinase/endothelial nitric oxide synthase (AMPK/eNOS) pathway.

Methods

Animals

Previous work has demonstrated that estrogen has an impact on angiogenesis after SCI (Samantaray et al., 2016; Ni et al., 2018), and thus we used male mice to exclude these effects. Two-month-old (young group, 22–24 g, *n* = 27) and 18-month-old C57BL/6J (aged group, 32–38 g, *n* = 132) male, specific pathogen-free mice were used for the *in vivo* experiments, and another 10–12 C57BL/6 male mice (aged 8–12 weeks, 22–26 g) were used for *in vitro* experiments. All mice were acquired from the Experimental Animal Center of Xiangya Hospital, Central South University (license No. SYXK (Xiang) 2020-0019). All animal procedures were approved by the Animal Welfare and Ethics Committee of Xiangya Hospital, Central South University (approval No. 2020sydw0374) on July 4, 2020. All *in vivo* experiments were designed and reported according to the Animal Research: Reporting of *In Vivo* Experiments (ARRIVE) guidelines (Percie du Sert et al., 2020) housed in separate cages under a 12/12-hour light/dark cycle in a temperature-controlled environment (temperature 22–24°C; humidity 60–80%), with free access to water and food. The animals were subjected to a surgical procedure mimicking SCI, and the outcomes were assessed in a blinded manner. To explore the differences between young and aged mice, young and aged SCI mice were randomly divided into young sham, young SCI, aged sham, and aged SCI groups. For the metformin treatment experiment, aged SCI mice were randomly divided into phosphate buffered saline (PBS) and metformin treatment groups. For the compound C administration experiment, aged SCI mice were randomly divided into sham, metformin only, and metformin plus compound C treatment groups. The study timeline is shown in **Additional Figures 1–3**.

Contusive SCI model and experimental design

A modified Allen approach was used to construct the traumatic SCI mouse model (Allen, 1911; Ni et al., 2019). Briefly, the mice were anesthetized by intraperitoneal injection of xylazine (10 mg/kg; Topscience, Shanghai, China, Cat# T7046) and ketamine (80 mg/kg; Ketathesia, Henry Schein Animal Health, Dublin, OH, USA). An incision was made on the back midline, followed by laminectomy at the T10 level. Then, a 10-g weight was applied to the dorsal surface of the exposed spinal cord dorsal surface using a modified Allen weight-drop apparatus set to a vertical height of 15 mm. The mouse bladders were emptied manually twice a day until normal voiding activity was recovered. Metformin (MedChemExpress, Monmouth Junction, NJ, USA, Cat# HY-B0627) was diluted to 100 mg/mL. The injured mice were injected intraperitoneally with metformin (100 mg/kg per day) and compound C (20 mg/kg per day; MedChemExpress, Cat# HY-13418A), an AMPK inhibitor, from 3 days post-SCI until the mice were sacrificed. PBS (20 µL; Solarbio, Beijing, China, Cat# P1010) was used as the vehicle-only control. Behavioral parameters were evaluated by Basso Mouse Scale (BMS) and tactile allodynia 24 hours after each daily dose of metformin and compound C.

Neurological assessment

The neurological assessment was based on motor and sensory tests post-SCI. The BMS hindlimb locomotor scale was used to assess recovery of hindlimb motor function before SCI and 1, 3, 7, 14, 21, 28, 35, 42, and 56 days post-SCI, as previously described (Basso et al., 2006; Ni et al., 2019). The BMS scores ranged from 0 (complete paralysis) to 9 (normal hindlimb motor function). Two blinded, independent reviewers assessed hindlimb locomotor function, and the two scores were averaged to yield the final BMS score.

Von Frey filament test

The Von Frey filament test was carried out using Semmes-Weinstein monofilaments (Stoetling Company, Dale, IL, USA), as previously described (Chaplan et al., 1994). Briefly, the filament was used to stimulate the plantar surface of the hindpaw. Rapid withdrawal or lifting of the stimulated hindpaw was considered a positive response. Paw withdrawal thresholds were measured as described previously (Ni et al., 2019). Tests were performed before surgery and 7, 14, 21, 28, 42, and 56 days post-SCI.

Electromyography

Motor-evoked potentials (MEPs) in the hindlimbs were assessed as described previously (Schlag et al., 2001). Briefly, 56 days post-SCI mice were anesthetized with xylazine (10 mg/kg) and ketamine (80 mg/kg). Then, stimulating electrodes (Chengdu Techman Instrument Co., Ltd., Chengdu, China) were placed on the skull over the cortical motor center, and recording electrodes were inserted in the contralateral hindlimb muscle. Electrical stimulation was performed at 3 V and 333 Hz and repeated every 2 seconds. The average amplitude of the MEP values and the latency period were recorded prior to SCI surgery and 56 days post-SCI.

Immunohistology

After anesthetization with xylazine (10 mg/kg) and ketamine (80 mg/kg), mice were perfused with normal saline and 4% paraformaldehyde (PFA) at different time points. The spinal cords were then collected and fixed with 4% PFA overnight, followed by immersion in a 30% sucrose solution and slicing into 16-µm transverse cryo-slices. For immunofluorescence staining, the spinal sections were incubated with anti-Ki67 (rabbit, 1:1000, Abcam, Cambridge, UK, Cat# ab15580, RRID: AB_443209) and anti-CD31 (goat, 1:100, R&D System, Inc., Minneapolis, MN, USA, Cat# AF3628,RRID: AB_2161028) primary antibodies overnight at 4°C. Then, the sections were incubated with secondary antibodies (donkey anti-goat IgG H&L (Alexa Fluor® 488), 1:400, Abcam, Cat# ab150129, RRID: AB_2687506; donkey anti-rabbit IgG H&L (Alexa Fluor® 594), 1:400, Abcam, Cat# ab150076, RRID: AB_2782993) for 1 hour at 4°C. Next, the sections were washed with PBS and mounted with Vectashield DAPI Hardmount (Vector Laboratories, Burlingame, CA, USA) for nuclear visualization. A fluorescence microscope (Carl Zeiss Axio Observer Z1, Oberkochen, Germany) was used to observe five random fields of view from every section, with 10 sections analyzed for every group. The percentage of the newly formed blood vessels (CD31-positive) and double-stained proliferated vascular endothelial cells (CD31 and Ki67 double-positive) was calculated for each field of view and averaged to generate a final value for each section. Representative 8-µm transverse spinal cord slices at the injury epicenter (*n* = 6 per group) were selected for hematoxylin-eosin staining to analyze the lesion size area, as previously described (Hu et al., 2016).

Three-dimensional microvascular visualization

The sample preparation for three-dimensional (3D) microvasculature imaging using an X-ray tomography microscope was performed as follows (*n* = 6 per group). In brief, 56 days post-SCI, young and aged mice from the SCI and sham groups were anesthetized with xylazine (10 mg/kg) and ketamine (80 mg/kg), followed by perfusion with normal saline and 4% PFA and injection of a contrast medium mixture (Microfil, MV-122, Flow Tech, Carver, MA, USA) into the ascending aorta. Then, the spinal cords were harvested, fixed in 4% PFA, and prepared for 3D microvasculature scanning. A ZEISS Xradia 410 Versa (Carl Zeiss XRM, Pleasanton, CA, USA) was employed to perform high-resolution and contrast XRM non-destructive 3D submicron imaging using a unique dual-stage process based on synchrotron-caliber optics followed by geometric magnification. The prepared spinal cord samples were scanned for 3 ms with the X-ray tube set to 40 kV and 10 kW. A pre-warm up procedure of 801 projections was performed, followed by 3001 projections of the target tissue. The image resolution was set at 3.25 µm/pixel. After scanning, all images were transformed into raw tiff format. VG studio Max 3.0 software (Volume Graphics, Heidelberg, Germany) was used to generate 3D images and analyze 3D vessel morphological parameters.

Footprint analysis

Footprint analysis was used to evaluate the hindlimb motor functional recovery before SCI surgery and 56 days post-SCI. Each animal's front and hind paws were dyed blue and red, respectively, and the animal was then placed on the runway paper (7.5 cm × 100 cm), where they walked from one end to the other as trained. The footprints were then scanned and analyzed using Image-Pro Plus 7.0 software (Media Cybernetics, Rockville, MD, USA).

Isolation and culturing of spinal cord microvascular endothelial cells

Primary mouse spinal cord microvascular endothelial cells (SCMECs) were isolated as described previously (Ruck et al., 2014). Briefly, the mice were anesthetized with xylazine (10 mg/kg) and ketamine (80 mg/kg) and then sacrificed by cervical dislocation (Ruck et al., 2014). The thoracic spinal cord was removed, minced, and digested with 0.1% (v/v) collagenase type II (Sigma-Aldrich, Burlington, MA, USA) in 10 mL Dulbecco's modified Eagle medium (DMEM; Gibco, Invitrogen, Paisley, UK) for an hour at 37°C on an orbital shaker. To remove myelin, the digested spinal cord tissue was centrifuged, and the pellet was resuspended into 20% bovine serum albumin-DMEM (20 mL, w/v), followed by 20 minutes of centrifugation at 3000 × *g* and 4°C. Next, the pellet was resuspended in 0.1% collagenase/dispase (Sigma, Burlington, MA, USA) in DMEM (10 mL), followed by 1 hour of digestion on the orbital shaker at 37°C. The solution was then centrifuged and, after rinsing, the pellet was resuspended twice with DMEM. The isolated SCMECs were inoculated onto endothelial cell medium plates supplemented with low-glucose DMEM, heparin (MedChemExpress, Cat# HY-17567A), 20% fetal bovine serum (Gibco), basic fibroblast growth factor (Peprotech, Cranbury, NJ, USA), and epidermal growth factor (Sigma) and used to conduct the following experiments.

Transwell migration assay
A 24-well Transwell chamber (pore size, 8 mm; Corning Incorporated, Corning, NY, USA) was used to evaluate the effect of metformin on SCMEC migration in the exponential growth phase. Trypsin was used to digest the SCMEC to create a cell suspension. Next, 2×10^5 cells/mL was added to the upper chamber, which contained DMEM (Gibco) supplemented with 1% fetal bovine serum, while medium containing 10% fetal bovine serum (600 μL) was introduced into the lower chamber. Thereafter, metformin at diverse doses (0.5, 1, 2, or 4 mM) and compound C (1 μM) were added into the bottom chamber. After incubation for 24 hours, the cells that had migrated to the bottom surface of the lower chamber were fixed in 4% PFA for 20–30 minutes, followed by 10 minutes of staining with 0.1% crystal violet. The vertically migrated SCMECs in five randomly chosen visual fields were quantified using Image-Pro Plus 7.0 software.

Scratch migration assay and tube formation assay
SCMECs were cultivated in six-well plates. When the cells reached 90% confluency, a scratch was made in the monolayer using a 200-μL pipette tip, and 200 μL metformin at different concentrations (0.5, 1, 2, and 4 mM) and compound C (1 μM) were added. At 0, 6, and 12 hours following treatment, a light microscope (CKX41; Olympus Corporation, Tokyo, Japan) was used to obtain images. The wound width was measured as described previously (Ni et al., 2019).

An *in vitro* angiogenesis assay tube formation kit (Cultrex, Trevigen, Inc., Gaithersburg, MD, USA) was used to evaluate tube formation after 24 hours. Briefly, SCMECs (2×10^4/well) were inoculated into wells containing 100 μL Matrigel, followed by treatment with different concentrations of metformin. The wound closure length, total branching length, and number of mesh extensions were calculated using Image-Pro Plus 7.0 software.

Western blot assay
Activation of the AMPK/eNOS pathway has been shown to have a beneficial effect on endothelial cells after metformin treatment. Spinal cord tissues were obtained at 7 days post-SCI and lysed using a radioimmunoprecipitation assay lysis buffer (Beyotime, Shanghai, China), and protein concentrations were measured using a bicinchoninic acid protein assay kit according to the manufacturer's instructions (Bio-Rad, Hercules, CA, USA). Proteins were separated by 10% sodium dodecyl sulfate-polyacrylamide gel electrophoresis, followed by transfer to a polyvinylidene fluoride membrane. The membrane was blocked with 5% milk in Tris-buffered saline with Tween. The membrane was then incubated overnight at room temperature (22–25°C) with antibodies against AMPK (rabbit, 1:500, Wanleibio, Shenyang, China, Cat# WL02254), phosphor-AMPK (p-AMPK; rabbit,1:500, Wanleibio, Cat# WL05103), eNOS (rabbit, 1:500; Wanleibio, Cat# WL01789), and phosphor-eNOS (p-eNOS; rabbit, 1:1000, CST, Beverly, MA, USA, Cat# 9571, RRID: AB_329837). Then, a secondary antibody (goat anti-rabbit IgG H&L (horseradish peroxidase), 1:2000, Abcam, Cat# ab6721, RRID: AB_955447) was added, and the membrane was incubated for 1 hour at room temperature. Finally, enhanced chemiluminescence (Amersham Biosciences, Pittsburgh, PA, USA) was used for band visualization, and images were obtained using a gel documentation system (Bio-Rad Gel and Multi-Analyst version 1.1, Bio-Rad, Hercules, CA, USA). Image Lab 3.0 software (BioRad) was employed to quantify band intensities.

Quantitative polymerase chain reaction
We choose four angiogenesis-related genes—angiopoietin-1 (ANG-1), brain-derived neurotrophic factor (BDNF), connective tissue growth factor (CTGF), and vascular endothelial growth factor (VEGF) – to explore differences between the young and aged groups before and 7 days after SCI. Spinal cord samples (1 cm long) near the injury center were collected, and total RNA was extracted using TRIzol (Invitrogen, Carlsbad, CA, USA) according to the manufacturer's instructions. Complementary DNA was then prepared by reverse transcription of the total RNA using a PrimeScript RT reagent kit (Takara, Kusatsu, Japan). A QuantStudio™ 5 Real-time PCR system (Applied Biosystems, Carlsbad, CA, USA) was used to perform quantitative polymerase chain reaction (qPCR) using SYBR Premix Ex Taq (Takara) with the following conditions: 40 qPCR cycles and an annealing temperature of 60°C. Gene expression levels were determined by the $2^{-\Delta\Delta CT}$ approach (Livak and Schmittgen, 2001), using glyceraldehyde phosphate dehydrogenase (GAPDH) as a housekeeping gene. The qPCR primer sequences are as follows: VEGF: forward, 5′-CTG TCT AAT GCC CTG GAG CC-3′, and reverse, 5′-ACG CGA GTC TGT GTT TTT GC-3′; ANG-1: forward, 5′-CAG CAC GAA GGA TGC TGA TA-3′, and reverse, 5′-TTA GAT TGG AAG GGC CAC AG-3′; BDNF: forward, 5′-ATG ACC ATC CTT TTC CTT ACT-3′, and reverse, 5′-CTA TCT TCC CCT TTT AAT GGT-3′; CTGF: forward, 5′-GTC TTC ACA CTG GTG CAG CC-3′, and reverse, 5′-ACT GGA AGA CAC ATT TGG CC-3′; GAPDH: forward, 5′-AGA AAA ACC TGC CAA ATA TGA TGA C-3′, and reverse, 5′-TGG GTG TCG CTG TTG AAG TC-3′.

Statistical analysis
No statistical methods were applied to predetermine the sample size. However, more animals were used in this study than in a previous publication (Arifin and Zahiruddin, 2017). No animals or data points were excluded from the analysis. The evaluators were blinded to the group assignments. GraphPad Prism 8.0.2 (GraphPad Software, San Diego, CA, USA, www.graphpad.com) was used to perform the statistical analyses. All the data were first tested for normality based on the Shapiro-Wilk test. All data are represented using means ± standard error of the mean (SEM). Two-tailed Student's *t*-test was adopted for comparison between two groups, whereas one-way analysis of variance followed by Tukey's multiple comparisons test was performed to compare multiple groups. $P < 0.05$ was considered to indicate statistical significance.

Results

Aging delays functional recovery and pathological outcomes in SCI
To assess how aging affects neurological recovery after SCI, three behavioral tests were implemented to analyze the differences between young and aged mice. As presented in **Figure 1A** and **B**, the BMS score and subscore were not significantly different between young and aged mice before SCI but trended toward recovery in both young and aged mice after SCI (**Figure 1A** and **B**). However, the aged SCI mice had markedly lower scores compared with young SCI mice starting at 7 days post-SCI. The aged group had a higher withdrawal threshold in response to mechanical stimuli post-SCI compared with the young group (**Figure 1C**). In addition, the aged group exhibited markedly impaired MEP amplitudes and latency periods 56 days post-SCI (**Figure 1D–F**).

Next, we examined the pathology of the aged spinal cord after SCI. First, we confirmed that the pathological changes 14 days post-SCI were consistent in the young and aged groups (**Additional Figure 4**) and found that the area of the lesion tissue around the injury site was larger in aged mice compared with young SCI mice at the same time point. Next, we explored the pathology at 56 days post-SCI. As **Figure 1G–H** shows, the area of the lesion around the injury site was larger in aged mice compared with young SCI mice at this time point and, conversely, there was less healthy spinal cord tissue in aged mice compared with young mice post-SCI (**Figure 1I**). Moreover, footprint analysis revealed that stride length and paw rotation were severely impaired in aged mice compared with young mice post-SCI (**Figure 1J–L**). Taken together, these findings imply that pathological changes in the spinal cord are worse, and neurological functional recovery is more impaired, in aged mice compared with young mice post-SCI.

Vascular regeneration is impaired in aged mice after SCI
To determine whether the poor recovery in aged mice post-SCI was due to impaired angiogenesis, the blood vessels were visualized by immunostaining. As presented in **Figure 2A** and **B**, the aged mice exhibited a lower percentage of newly formed blood vessels (CD31-positive cells) at 56 days post-SCI compared with young mice. Because the greatest degree of vascular proliferation occurs at 7 days post-injury (Cao et al., 2017), this time point was selected to evaluate the proliferation of SCMECs isolated from aged and young mice. As **Figure 2C** and **D** shows, immuno-stained spinal cord slices taken 7 days post-SCI exhibited substantially fewer proliferated endothelial cells (Ki-67 and CD31 double-positive cells) in the aged group compared with the young group, suggesting that micro-vessel growth is attenuated in aged mice after SCI. Next, qPCR was conducted to analyze alterations in the mRNA expression levels of four angiogenesis-related genes (ANG-1, BDNF, CTGF, and VEGF) within injured spinal cord tissue from both groups. We found that ANG-1, BDNF, CTGF, and VEGF mRNA levels were markedly higher in the young group compared with the aged group at 7 days post-SCI (**Figure 2E–H**). Then, comparative X-ray microscope tomography imaging of the spinal cord microvasculature was performed to analyze specific 3D morphological alterations post-SCI in both young and aged mice. As shown in **Figure 3A**, visualization of the 3D architecture of the spinal cord micro-vessel networks enabled accurate quantification of vascular segment, vascular volume fractions, and vascular bifurcation. **Figure 3A** depicts 3D images of the spinal cord microvasculature at the T10 levels in control and injured young and aged mice. In the control animals, the quantitative parameters of the spinal cord vasculature were similar in aged mice and young mice. However, at 56 days post-SCI, the vascular parameters of the spinal cord were lower in aged mice than in young mice (**Figure 3B–D**), which was consistent with our immunostaining results. Collectively, these data suggest that the impaired neurological functional recovery observed in the aged mice may be associated with impaired vascular regeneration.

Metformin promotes SCMEC migration and tube formation *in vitro*
Metformin has anti-aging and pro-angiogenic effects in the context of several diseases (Takahashi et al., 2015; Barzilai et al., 2016; Yu et al., 2016; Piskovatska et al., 2020). To determine whether metformin promotes angiogenesis after SCI, we first explored its effects on SCMECs *in vitro*. First we isolated SCMECs and confirmed their identity by light microscopy and immunofluorescence (**Additional Figure 5**). Seven days after seeding, SCMEC colonies appeared (**Additional Figure 5A**), and CD31 immunofluorescence was detected (**Additional Figure 5B**). Next, we performed scratch and Transwell assays and found that metformin enhanced SCMEC migration horizontally and vertically in a concentration-dependent manner, as shown in **Figure 4A–D**. Additionally, SCMEC canaliculization increased markedly as the metformin concentration increased, as indicated by the tube formation assay (**Figure 4E–G**). Of note, 4 mM metformin induced less SCMEC migration and tube formation than 2 mM metformin, suggesting that 2 mM may be the optimal concentration of metformin for promoting SCMEC-mediated angiogenesis.

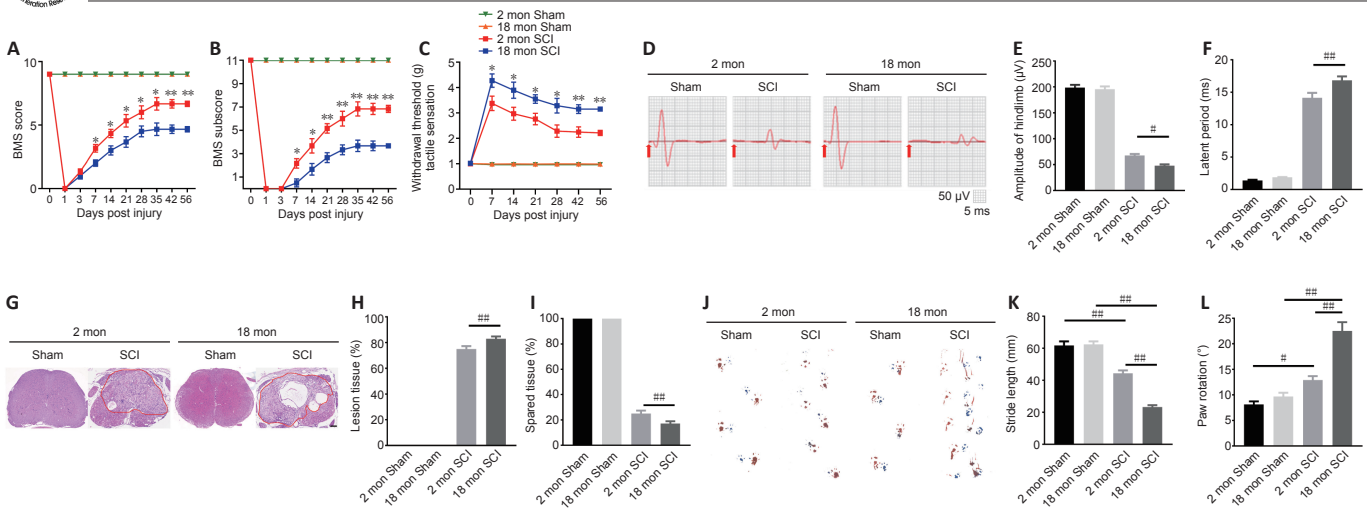

Figure 1 | **Aging attenuates neurological functional recovery and tissue repair after SCI.**
(A, B) Functional evaluation of locomotor recovery in aged and young mice post-injury as assessed by BMS scoring over 56 days. (C) Analysis of sensory function based on withdrawal threshold in young and aged mice post-SCI. (D) Representative electrophysiological traces from young and aged mice after sham surgery and SCI at 56 days. The aged mice exhibited lower MEP amplitudes and longer latency periods compared with young mice after SCI. (E, F) Quantification of amplitudes and latent periods in young and aged mice post-SCI. (G) Representative H&E-stained transverse sections at the injury epicenter from the different groups. The aged mice exhibited more severe lesions and less healthy tissue compared with young mice after SCI. Red lines indicate the lesion areas. Scale bar: 200 μm. (H, I) Quantification of lesioned tissue and healthy tissue areas in young and aged mice post-SCI. (J) Representative images of footprint analysis of young and aged mice 56 days after sham surgery or SCI. The aged mice exhibited shorter stride length and more paw rotation compared with young mice after SCI. (K, L) Quantification of the stride length and paw rotation data shown in J. The data are presented as the mean ± SEM (n = 6 per group). *P < 0.05, **P < 0.01, *vs*. aged mice post-SCI; #P < 0.05, ##P < 0.01 (two-tailed Student's t-test [A–C, H, and I], or one-way analysis of variance followed by Tukey's multiple comparisons test [E, F, K, and L]). BMS: Basso Mouse Scale; H&E: hematoxylin-eosin; MEP: motor evoked potential; SCI: spinal cord injury.

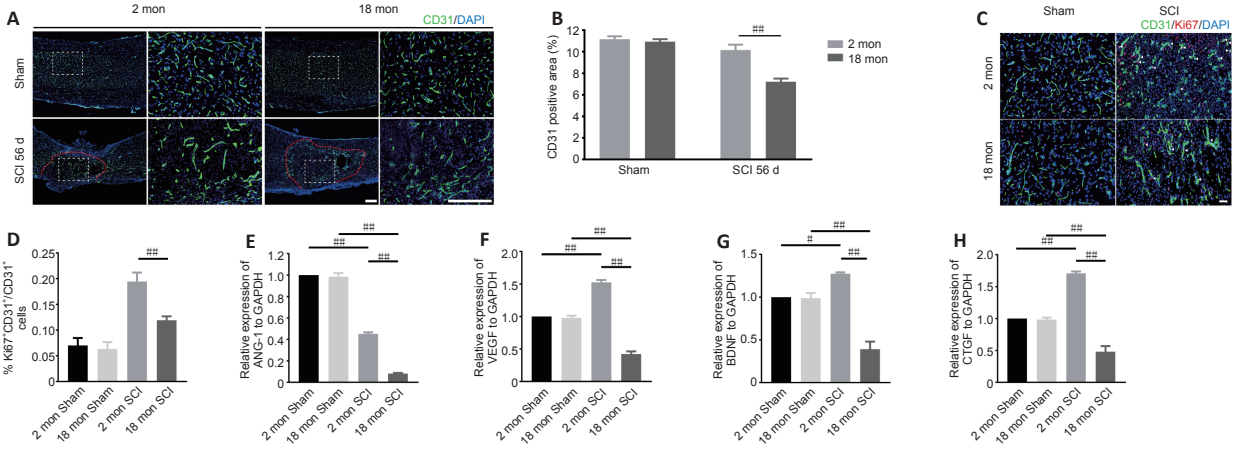

Figure 2 | **Aging results in reduced vessel numbers and vascular proliferation after SCI.**
(A) Representative images of spinal cord blood vessels immunostained with CD31 (green-Alexa Fluor® 488) in young and aged mice post-SCI. The aged mice exhibited less vascular density compared with the young mice after SCI. Red lines indicate the epicenter of the injury site. (B) Quantification of the labeled blood vessels in the different groups. (C) Representative images of blood vessels immunostained with CD31 (green-Alexa Fluor® 488) and Ki67 (red-Alexa Fluor® 594) in the spinal cord of young and aged mice at 7 days post-SCI. Vascular regeneration was impaired in aged mice compared with young mice after SCI. Scale bars: 50 μm. (D) Quantification of $CD31^+Ki67^+$ cells in the spinal cords of mice from the different groups. (E–H) Changes in ANG-1, VEGF, BDNF, and CTGF mRNA expression 7 days post-SCI in young and aged mice as determined by quantitative polymerase chain reaction. The data are presented as the mean ± SEM (n = 3 per group). #P < 0.05, ##P < 0.01 (two-tailed Student's t-test [B]), or one-way analysis of variance followed by Tukey's multiple comparisons test [D–H]). ANG-1: Angiopoietin-1; BDNF: brain-derived neurotrophic factor; CTGF: connective tissue growth factor; SCI: spinal cord injury; VEGF: vascular endothelial growth factor.

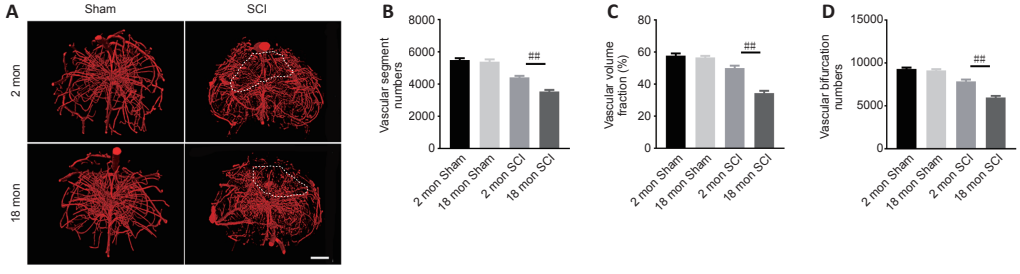

Figure 3 | **Three-dimensional visualization of microvasculature changes in the spinal cords of young and aged mice post-SCI.**
(A) Representative three-dimensional images of spinal cord microvasculature in young and aged mice post-SCI taken by X-ray microscopy. The aged mice exhibited fewer vascular parameters in the area of interest compared with young mice after SCI. White dashed lines indicate the area of interest. Scale bar: 200 μm. (B–D) Three-dimensional quantitative analysis of spinal cord microvasculature morphometric data in normal and post-spinal cord injury young and aged mice. The data are presented as the mean ± SEM (n = 6 per group). ##P < 0.01 (one-way analysis of variance followed by Tukey's multiple comparisons test). SCI: Spinal cord injury.

Metformin promotes neurological functional recovery and tissue repair in aged mice after SCI

To better illustrate metformin's role in tissue repair and functional recovery in aged mice after SCI, we systematically evaluated the recovery of hindlimb motor function. First, the BMS score and subscore were determined to assess the recovery of neurological function in the metformin and PBS groups. As shown in **Figure 5A** and **B**, the aged mice treated with metformin had markedly higher BMS scores and subscores (starting at 7 days post-SCI) and enhanced motor function than the aged mice treated with PBS post-SCI. Additionally, the aged mice treated with metformin had lower withdrawal thresholds in response to mechanical stimulus than the aged mice treated with PBS post-SCI, suggesting that metformin may promote sensory recovery in aged mice post-SCI (**Figure 5C**). To better evaluate the role of metformin function in the recovery of motor function, electrophysiological testing was carried out. As shown in **Figure 5D**, treatment with metformin lead to clearly elevated MEP amplitudes and markedly shorter latency periods relative to treatment with PBS at 56 days post-injury (**Figure 5E** and **F**). H&E staining showed that the area of spinal cord tissue with normal integrity at the injury site was markedly increased in the metformin group compared with the PBS group (**Figure 5G** and **H**), and the area of injured tissue was dramatically decreased in the metformin group compared with PBS group (**Figure 5I**). Furthermore, footprint analysis showed that treatment with metformin resulted in a longer stride length and less paw rotation in aged mice at 56-day post-SCI relative to the PBS group (**Figure 5J–L**). These results suggest that metformin is neuroprotective and significantly improves tissue repair and neurological functional recovery in aged mice post-SCI.

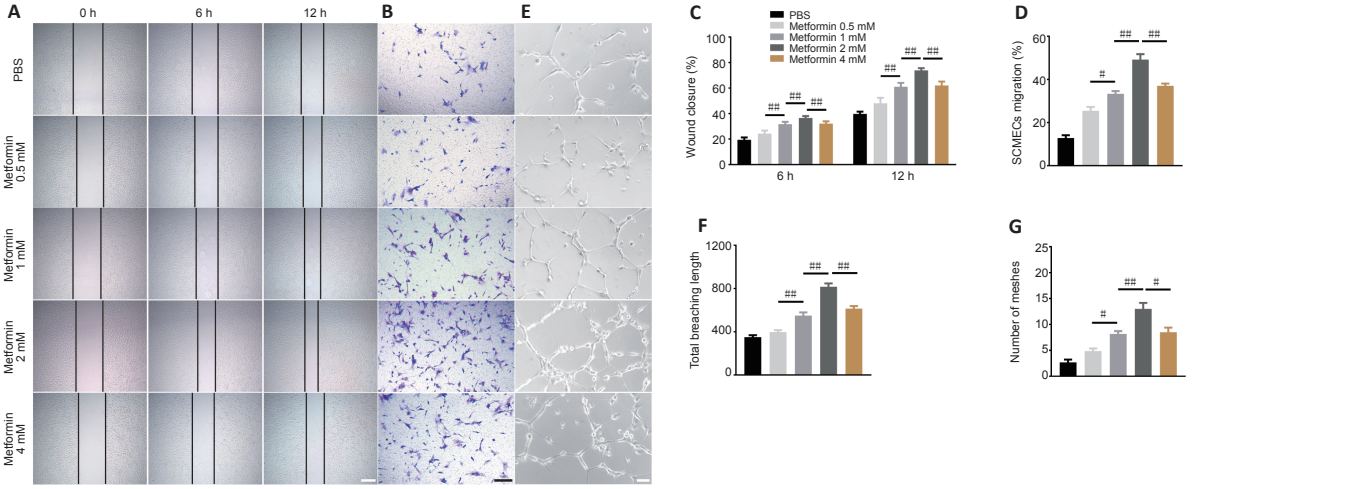

Figure 4 | **Metformin promotes SCMEC-mediated angiogenesis *in vitro*.**

(A) Representative images of wound-healing experiment by SCMECs treated with different doses of metformin or PBS. Metformin markedly increased wound healing by SCMECs, (B) Representative images of the results from a Transwell experiment in which SCMECs were treated with different doses of metformin or PBS. Metformin dramatically increased SCMEC migration. (C) Quantification of the wound closure results shown in A. (D) Quantification of the SCMEC migration results shown in B. (E) Representative images of tube formation by SCMECs treated with different doses of metformin or PBS. A marked increase in tube formation by SCMECs was observed after administration of different doses of metformin. Scale bars: 300 μm in A, 200 μm in B, 100 μm in E. (F, G) Quantification of the total branching length and tube mesh extension data shown in E. The data are presented as the mean ± SEM (n = 6 per group). #P < 0.05, ##P < 0.01 (one-way analysis of variance followed by Tukey's multiple comparisons test). PBS: Phosphate buffer saline; SCMECs: spinal cord microvascular endothelial cells.

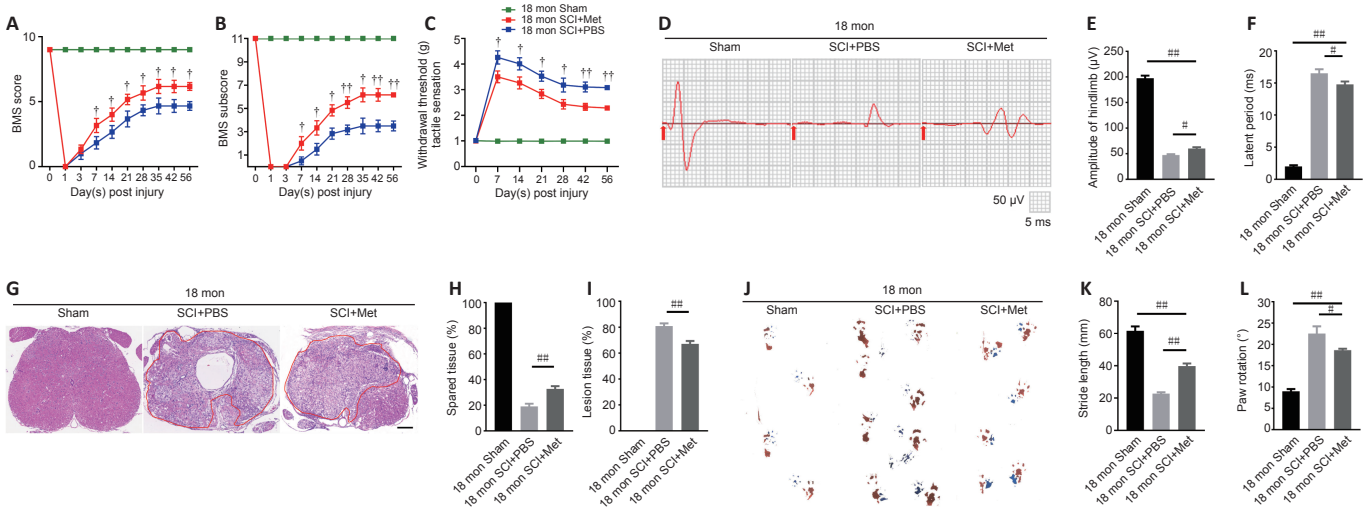

Figure 5 | **Metformin promotes neurological functional recovery and tissue repair after SCI in aged mice.**

(A, B) Functional evaluation of locomotor recovery in aged mice treated with PBS or metformin and in the sham group as determined by BMS scoring over 56 days. Metformin markedly promoted hindlimb functional recovery in aged mice after SCI compared with the PBS group. (C) Sensory function analysis based on withdrawal threshold in aged mice treated with PBS or metformin and the sham group post-injury. Metformin markedly promoted hindlimb sensory recovery in aged mice after SCI compared with the PBS group. (D) Representative electrophysiological traces from aged mice treated with PBS or metformin and the sham group post-injury at 56 days. Metformin markedly enhanced MEP amplitude and latency in aged mice after SCI compared with the PBS group. (E, F) Quantification of amplitudes and the latency period in aged mice treated with PBS or metformin and the sham group. (G) Representative H&E-stained transverse sections from the injury epicenter from the different groups. The aged mice exhibited smaller lesions and more healthy tissue compared with the PBS group after SCI. Red lines indicate the lesion area. Scale bar: 200 μm. (H, I) Quantification of the health and lesioned tissue area data shown in G. (J) Representative images of footprint analysis of aged mice before surgery and 56 days post-SCI treated with PBS or metformin. Longer stride length and less paw rotation were observed after metformin administration. (K, L) Quantification of the stride length and paw rotation data shown in J. The data are presented as the mean ± SEM (n = 6 per group). #P < 0.05, ##P < 0.01; †P < 0.05, ††P < 0.01, *vs.* aged mice post-SCI with PBS treatment (two-tailed Student's t-test [A–C], or one-way analysis of variance followed by Tukey's multiple comparisons test [E, F, H, I, K, and L]). BMS: Basso Mouse Scale; H&E: hematoxylin-eosin; MEP: motor evoked potential; PBS: phosphate buffer saline; SCI: spinal cord injury.

Metformin promotes angiogenesis in aged mice after SCI

Next, we asked whether the neuroprotective effect of metformin on SCI is due to its promotion of angiogenesis. Immunofluorescence analysis showed that metformin administration markedly increased the percentage of CD31-positive cells at the injury site in aged mice 7, 14, and 56 days after SCI compared with PBS administration (**Figure 6A** and **B**). Furthermore, treatment with metformin increased the percentage of CD31 and Ki67 double-positive cells in aged mice at 7 days post-SCI (**Figure 6C** and **D**).

To explore the molecular mechanism by which metformin promotes angiogenesis in aged mice post-SCI, we investigated the AMPK/eNOS pathway, which has been shown to have a beneficial effect on endothelial cells after treatment with metformin (Takahashi et al., 2015; Yu et al., 2016). The AMPK/eNOS pathway was markedly activated in the spinal cord of aged animals 7 days post-SCI after treatment with metformin, as confirmed by western blotting analysis (**Figure 6E–G**). Collectively, these results suggest that activation of the AMPK/eNOS pathway may be involved in the metformin-mediated angiogenesis observed in aged mice post-SCI.

Inhibition of the AMPK/eNOS pathway reverses the pro-angiogenic effects of metformin on SCMECs

To determine whether the AMPK/eNOS pathway affects SCMEC function after treatment with metformin, AMPK expression was inhibited *in vitro* using compound C. First, we confirmed by western blotting that activation of the AMPK/eNOS pathway was blocked by treatment with compound C (**Figure 7A–C**). Then, we performed scratch and Transwell assays and found that compound C abolished the horizontal and vertical SCMEC migration caused by treatment with 2 mM metformin (**Figure 7D–G**). Compound C also robustly repressed SCMEC canaliculization, as determined by quantification of tube formation (**Figure 7H–J**). These findings indicate that inhibition of the AMPK/eNOS pathway attenuated the pro-angiogenic effects of metformin on SCMECs *in vitro*.

Inhibition of the AMPK/eNOS pathway abolishes the beneficial effect of metformin on functional recovery and angiogenesis in aged SCI mice

As described above, the AMPK inhibitor compound C attenuates the ability of metformin to promote SCMEC migration and tube formation *in vitro*. To explore the effect of compound C on neurological functional recovery and angiogenesis, next we intraperitoneally injected compound C and metformin into aged mice after SCI. We first asked whether compound C affects the tissue architecture of the spinal cord before SCI and 56 days post-SCI. As shown in **Additional Figure 6**, treatment with compound C did not affect the tissue architecture of spinal cord before or after SCI in aged mice. Next, we conducted behavioral assessments (the BMS scoring system and Von-Frey test) over an 8-week observation period to evaluate motor and sensory functional recovery. As shown in **Figure 8A** and **B**, BMS scores and subscores were clearly lower in the metformin plus compound C treatment groups than in the metformin only groups beginning at 7 days post-SCI (**Figure 8A** and

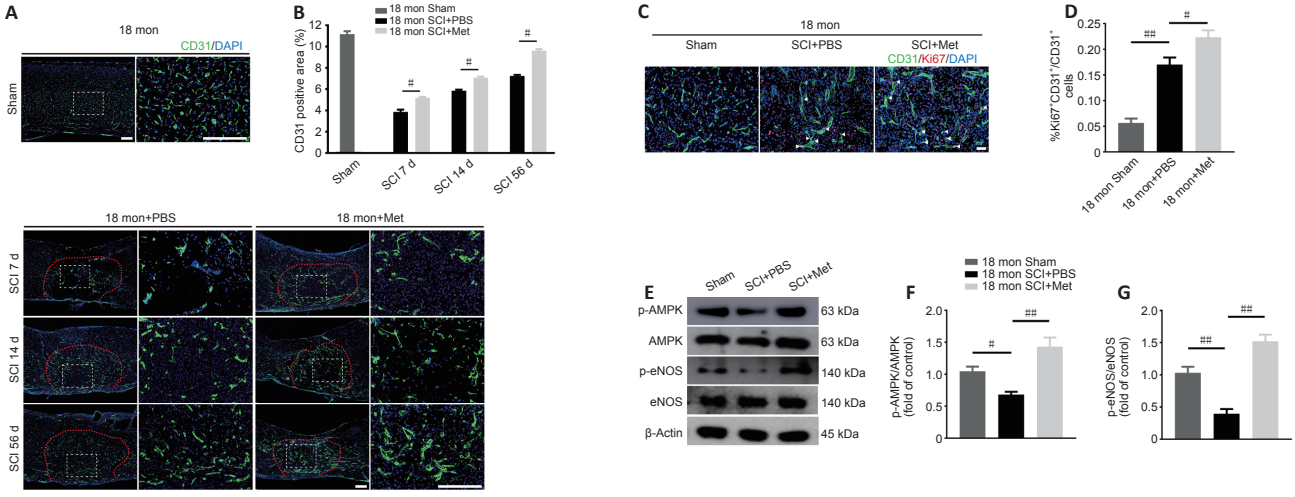

Figure 6 | **Metformin promotes vascular regeneration in aged mice post-SCI.**

(A) Representative image of spinal cord blood vessels immunostained for CD31 (green-Alexa Fluor® 488) in aged mice treated with metformin (100 mg/kg) or PBS. Metformin markedly enhanced vascular density in aged mice after metformin administration compared with the PBS group. Red lines indicate the epicenter of the injury site. (B) Quantification of the CD31-labeled blood vessels. (C) Representative images of blood vessels immunostained with CD31 (green-Alexa Fluor® 488) and Ki67 (red-Alexa Fluor® 594) in the sham mice and in aged metformin-treated and PBS-treated mice 7 days post-SCI. Metformin promoted more vascular regeneration in aged mice after metformin administration compared with the PBS group. Scale bars: 150 μm in A, 50 μm in C. (D) Quantification of $CD31^+Ki67^+$ cells in the different groups. (E) Representative western blot images of p-AMPK, AMPK, p-eNOS, and eNOS expression in aged mice 7 days post-SCI. (F, G) Quantification of p-AMPK/AMPK and p-eNOS/eNOS expression in aged mice or the sham group treated with metformin or PBS. The data are presented as the mean ± SEM (n = 3 per group). #P < 0.05, ##P < 0.01 (two-tailed Student's t-test [B]), or one-way analysis of variance followed by Tukey's multiple comparisons test [D, E–G]). PBS: Phosphate buffer saline; SCI: spinal cord injury.

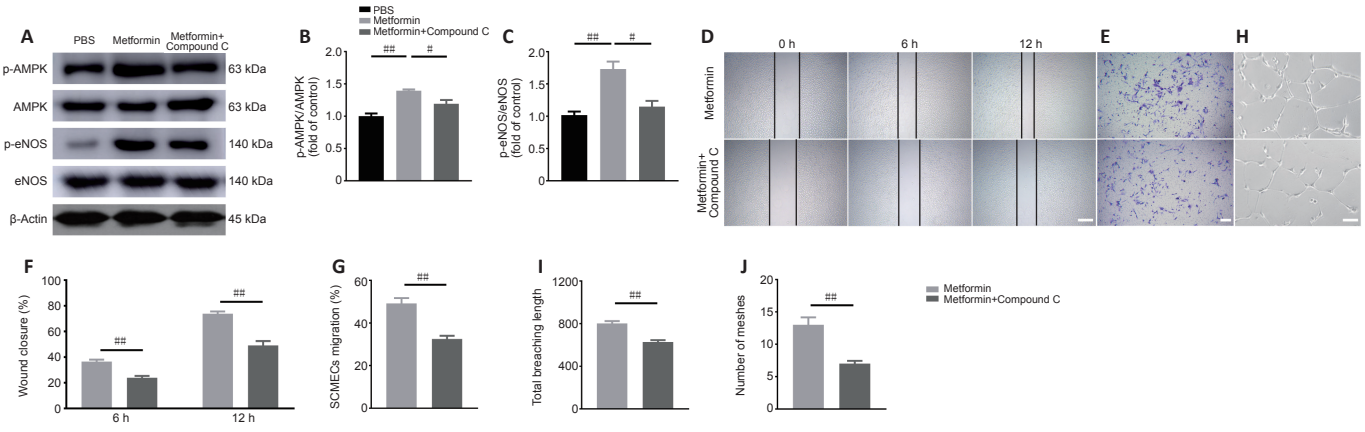

Figure 7 | **Inhibition of the AMPK/eNOS pathway attenuates the beneficial effects of metformin on angiogenesis in SCMECs *in vitro*.**

(A) Representative western blot images of p-AMPK, AMPK, p-eNOS, and eNOS expression in SCMECs treated with metformin, metformin + compound C or PBS (n = 3 per group). (B, C) Quantification of p-AMPK/AMPK and p-eNOS/eNOS expression in SCMECs subjected to different treatments. (D) Representative images of wound healing by SCMECs treated with PBS, metformin, or metformin + compound C. (E) Representative images of Transwell analysis of SCMECs treated with PBS, metformin, or metformin + compound C. (F) Quantification of the wound closure data shown in D. (G) Quantification of the migration data shown in E. (H) Representative images of tube formation by SCMECs treated with PBS, metformin, or metformin + compound C. Scale bars: 300 μm in D, 200 μm in E, 100 μm in H. (I, J) Quantification of the total branching length and tube mesh extension data shown in H. The data are presented as the mean ± SEM (n = 3 per group in A–C, n = 6 per group in D–J). #P < 0.05, ##P < 0.01 (one-way analysis of variance followed by Tukey's multiple comparisons test (B, C), or two-tailed Student's t-test (F–J)). AMPK: Adenosine monophosphate-activated protein kinase; Compound C: an AMPK inhibitor; eNOS: endothelial nitric oxide synthase; p-AMPK: phosphor-AMPK; p-eNOS: phosphor-eNOS; PBS: phosphate buffer saline; SCMECs: spinal cord microvascular endothelial cells.

B). The withdrawal thresholds in response to mechanical stimuli were also increased in aged mice treated with metformin plus compound C relative to those treated with metformin only, suggesting that compound C abolished the beneficial effect of metformin on motor and sensory functional recovery in aged mice post-SCI (**Figure 8C**). Electrophysiological analysis showed that, in aged mice post-SCI, the combined treatment group had markedly worsened MEP amplitudes and latency periods compared with metformin only group (**Figure 8D–F**). In addition, histological analysis revealed less preservation of spinal cord integrity following combined treatment compared with treatment with metformin only (**Figure 8G** and **H**). The opposite was true for the lesioned area: the injured area of the spinal cord following treatment with metformin plus compound C was markedly increased compared with metformin only (**Figure 8I**). Furthermore, footprint analysis demonstrated that the aged mice treated with metformin had a much longer stride length and less paw rotation at 56 days post-SCI, while treatment with metformin plus compound C inhibited hindlimb functional recovery (**Figure 8J–L**). Thus, compound C inhibits the ability of metformin to promote neurological functional recovery post-SCI in aged mice.

To further explore the role of the AMPK/eNOS pathway in metformin-promoted angiogenesis *in vivo*, we used immunofluorescence to detect vascular formation and endothelial cell proliferation following treatment with metformin plus compound C. Both the vascular ratio and endothelial cell proliferation at the injury site were reduced after treatment with compound C compared with treatment with metformin alone in aged mice after SCI (**Figure 9A–D**). These results suggest that compound C inhibits the ability of metformin to promote angiogenesis and neurological functional recovery in aged mice post-SCI.

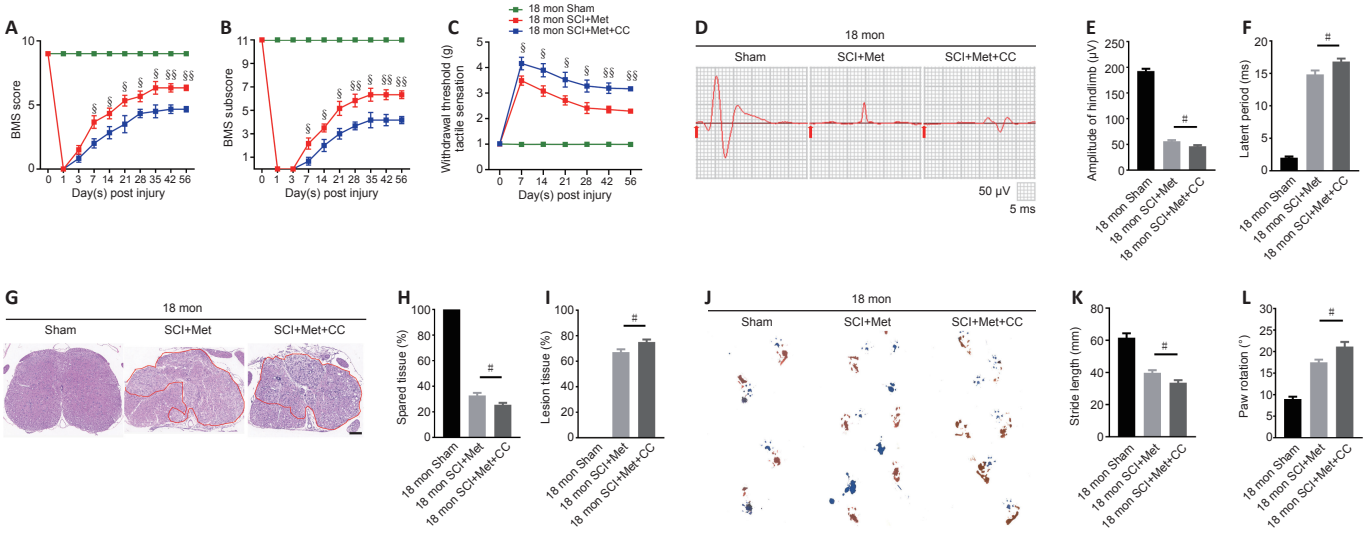

Figure 8 | Inhibition of the AMPK/eNOS pathway abolishes the beneficial effects of metformin on functional recovery in the aged mice following injury.
(A, B) Functional evaluation of locomotor recovery in aged mice treated with metformin or metformin + compound C and the sham group as determined by BMS scoring over a 56-day period. Compound C reversed the beneficial effects of metformin on hindlimb functional recovery in aged mice after SCI. (C) Sensory functional analysis based on withdrawal threshold in aged mice treated with metformin or metformin + compound C and the sham group post-injury. (D) Representative electrophysiological traces in aged mice treated with metformin only or metformin + compound C post-injury at 56 days and in the sham group. The metformin + compound C group exhibited more severe MEP disruption compared with the metformin only group. (E, F) Quantification of the amplitude and latency period data from the different groups as shown in D. (G) Representative hematoxylin-eosin-stained transverse sections from the injury epicenter among the different groups. The metformin plus compound C group exhibited more severe pathological changes. Red lines indicate the lesion area. Scale bar: 200 μm. (H, I) Quantification of the healthy and lesioned tissue data shown in G. (J) Representative images of footprint analysis of aged mice before surgery and 56 days post-SCI treated with metformin or metformin + compound C. The metformin plus compound C group exhibited more severely impaired hindlimb motor recovery than the metformin only group based on footprint analysis. (K, L) Quantification of the stride length and paw rotation data shown in J. The data are presented as the mean ± SEM (n = 6 per group). #P < 0.05; §P < 0.05, §§P < 0.01, *vs.* aged mice post-SCI with metformin + compound C treatment (two-tailed Student's t-test). AMPK: Adenosine monophosphate-activated protein kinase; BMS: Basso Mouse Scale; CC: Compound C, an AMPK inhibitor; eNOS: endothelial nitric oxide synthase; Met: metformin; MEP: motor evoked potential; SCI: spinal cord injury.

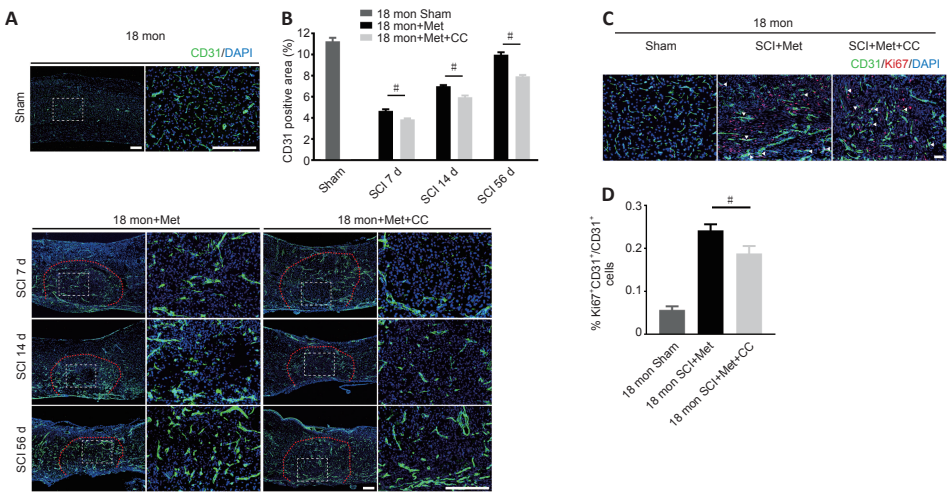

Figure 9 | Inhibition of the AMPK/eNOS pathway reverses the beneficial effects of metformin on angiogenesis in aged mice following injury.
(A) Representative images of spinal cord blood vessels immunostained with CD31 (green-Alexa Fluor® 488) in aged mice treated with metformin (100 mg/kg) or metformin + compound C. The metformin + compound C group exhibited less vascular density than the metformin only group. Red lines indicate the epicenter of the injury site. (B) Quantification of the CD31-labeled blood vessels. (C) Representative images of blood vessels immunostained with CD31 (green-Alexa Fluor® 488) and Ki67 (red-Alexa Fluor® 594) in the sham group and in aged mice treated with metformin or metformin + compound C at 7 days post-SCI. The metformin + compound C group exhibited less vascular regeneration than the metformin only group. Scale bars: 150 μm in A, 50 μm in C. (D) Quantification of $CD31^+Ki67^+$ cells. The data are presented as the mean ± SEM (n = 6 per group). #P < 0.05 (two-tailed Student's t-test). AMPK: Adenosine monophosphate-activated protein kinase; CC: Compound C, an AMPK inhibitor; DAPI: 4′,6-diamidino-2-phenylindole; eNOS: endothelial nitric oxide synthase; Met: metformin; SCI: spinal cord injury.

Discussion

The mammalian central nervous system has very low capacity for regeneration due to its limited regenerative plasticity (Hilton and Bradke, 2017; Tran et al., 2018). Neovascularization is therefore of paramount importance for the neuroparenchyma tissue survival (Figley et al., 2014). In the healthy spinal cord, vasculature provides nutrients and removes metabolic waste, and these processes play an important role in maintaining normal function. Therefore, promoting angiogenesis post-SCI is a promising therapeutic goal.

The mechanical forces involved in SCI, however, result in destruction of the vasculature, causing local hypoxia at the lesion epicenter. Angiogenesis initiates a few days post-SCI in response to hypoxia but regresses significantly around 14 days post-injury; thus, it cannot provide sufficient nutrition for SCI repair (Benton et al., 2008; Cao et al., 2017). All organs experience dynamic changes with aging (DiLoreto and Murphy, 2015; Ungvari et al., 2018), and recovery after SCI requires blood vessel growth. Nevertheless, it is unknown whether aging impacts angiogenesis after SCI.

Previous research demonstrated that ischemia-induced angiogenesis was attenuated in aged rats subjected to middle cerebral artery occlusion (Tang et al., 2016). In the current study, we found that the morphological parameters of the spinal cord vascular network differed in aged versus young mice subjected to SCI. Furthermore, we found that, while trauma-induced angiogenesis occurs in both young and aged mice after SCI, vessel regeneration is less robust in aged mice, which is consistent with findings from a previous study (Tang et al., 2016).

The functionality of the nervous system is dependent upon a normal blood supply (Figley et al., 2014), and therefore increased blood-vessel density is closely associated with improved functional outcomes after SCI. According to our results, in addition to reducing the angiogenic response in mice, aging limited the recovery of locomotive and sensory functions post-SCI. Therefore, our findings suggest that angiogenesis may influence nerve function recovery post-SCI.

Trauma-induced angiogenesis is regulated via complicated interactions among diverse molecules (Sinescu et al., 2010; Shi et al., 2017, 2018). Previous studies have characterized the many cellular events involved in angiogenesis after SCI. Importantly, remodeling of the functional vascular network is dependent on factors secreted by the local microenvironment after injury (Graumann et al., 2011; Kundi et al., 2013). Our observations revealed that angiogenesis is impaired in the aged spinal cord in response to trauma, although the molecular pathways that are reactivated under these pathological conditions and the effect of aging on angiogenesis at the cellular and subcellular levels remain largely unclear.

Ang-1, which is a main member of the angiopoietin family, promotes endothelial cell survival, sprouting, and tube formation, which are involved in both physiological and pathological angiogenesis processes (Isidori et al., 2016; Duran et al., 2021; Joussen et al., 2021). Unlike numerous other vascular growth factors, the expression of BDNF, which is a newly described meditator of endothelial cell survival and angiogenesis, is relatively restricted to central arteries (Donovan et al., 2000; Kermani and Hempstead, 2007; Wang et al., 2019). In addition to VEGF, CTGF plays a critical role in vessel homeostasis and angiogenesis (Brigstock, 2002; Ungvari et al., 2017). In our study, we found that these four angiogenesis-related genes (ANG-1, BDNF, CTGF, and VEGF) were upregulated after injury to the spinal cord tissue. However, it appears likely that this response may be impaired by aging, which could help explain the impaired vascular function and angiogenesis observed following injury in the elderly (Dumbrava et al., 2022; Riggin et al., 2022). It will be of great interest to elucidate exactly how these angiogenic factors are affected by aging process. Novel therapies that promote secretion of these factors into the local microenvironment may be conducive to regenerating blood vessels in elderly patients.

In addition to changes in local molecular factors that occur with aging, we speculate that other aging-related physiological changes in the vasculature could also affect vascular regeneration and neuronal integrity. Loss of stem cell activity with aging is likely to disrupt the regeneration process. Previous research has identified a resident vascular progenitor cell that localizes around blood vessels and could be capable of regenerating capillary networks (Pang et al., 2017). However, aging could impair the function of endothelial progenitor cells and inhibit their differentiation (Ungvari et al., 2018). In addition, endothelial cells undergo cellular senescence with aging, ceasing to proliferate and thus limiting the capacity to form new vasculature (Lähteenvuo and Rosenzweig, 2012; Ungvari et al., 2018). Our findings are consistent with those from a previous study (Tang et al., 2016). Future research may help define the underlying mechanisms of aging that impact angiogenesis. In addition, gaining a better understanding of the pathological changes that occur in the vasculature of aged mice after injury will help develop targeted therapeutic interventions for promoting angiogenesis in elderly patients. Pharmacological approaches that eliminate senescent endothelial cells could aid vessel regeneration and enhance the recovery of neurological function post-SCI in aged rodents.

Over the past decade, substantial progress has been made in treating SCI, although only a small number of treatment strategies have been successfully translated to the clinic, and these treatments only slightly improve functional recovery, especially among aged SCI patients. Given the aging of the global population, anti-SCI interventions for elderly patients are urgently needed. Over the past several years, increasing evidence has shown that metformin, a common hypoglycemic drug, has pleiotropic effects on several aging-related diseases and biological functions associated with aging (Chen et al., 2016; Piskovatska et al., 2020) and reduced risk of cancer (Kamarudin et al., 2019). Treatment with metformin may be a promising approach to achieving functional recovery post-SCI because it promotes improvement of a variety of biological functions. In several preclinical studies of SCI, metformin was shown to be capable of regulating autophagy and repressing inflammation and neuronal apoptosis, thus improving functional recovery after SCI, potentially through activation of the Wnt/β-catenin pathway (Wang et al., 2016; Zhang et al., 2017b, 2020). In addition, the administration of metformin enhances axon regeneration by reducing oxidative stress and stabilizing microtubules (Wang et al., 2020), indicating that it has substantial regenerative potential that could be helpful for the treatment of SCI. Moreover, metformin significantly prolongs longevity in mice by enhancing their overall health (Anisimov et al., 2010; Cabreiro et al., 2013). These effects not only emphasize the potential importance of metformin treatment in aging and in SCI treatment but also could open up new avenues for therapeutic developments in treating aged mice after SCI. In the current study, we found that metformin treatment significantly promotes vascular regeneration in aged mice after SCI, thereby enhancing tissue repair and recovery of hindlimb motor and sensory function. This finding highlights the role of metformin in regulating blood vessel formation, which enhance sensorimotor recovery and neuroplasticity.

AMPK, which is an important enzyme responsible for energy metabolism, is activated by metformin (Zhou et al., 2001; Musi et al., 2002). AMPK phosphorylates a number of enzymes, including acetyl-coenzyme A carboxylase, 3-hydroxy-3-methylglutaryl-coenzyme A reductase, glycogen synthase, and eNOS, which are associated with multiple biosynthetic reactions (Chen et al., 1999; Kahn et al., 2005; Long and Zierath, 2006). A previous report demonstrated that AMPK induces NO production by phosphorylating eNOS, thereby maintaining a functional balance in endothelial cells (Yuyun et al., 2018). In addition, activation of the AMPK/eNOS pathway is closely associated with vascular endothelial cell regeneration, particularly under hypoxic and ischemic conditions (Ikeda et al., 2012; Huang et al., 2015; Xu et al., 2015b; Ren and Luo, 2021). Metformin has also been reported to possibly activate the AMPK/eNOS pathway, thereby stimulating angiogenesis by endothelial progenitor cells in mice with diabetes (Yu et al., 2016) and promoting revascularization in an ischemic hindlimb mice model (Takahashi et al., 2015). These findings demonstrate the importance of metformin in angiogenesis, which is consistent with the current study, in which we found that activation of the AMPK/eNOS pathway may mediate metformin-induced angiogenesis in aged mice post-SCI. Administration of compound C abrogated the beneficial effects of metformin on angiogenesis *in vivo* and *in vitro*, indicating that metformin treatment promotes neurological functional recovery and angiogenesis in aged mice after SCI through the AMPK/eNOS pathway.

This study had several limitations. First, 18-month-old mice were used for the aged group, while, considering the demographic shift in patients with SCI, older mice (such as 22–24 months of age) may be more appropriate to explore angiogenesis and hindlimb motor recovery post-SCI. Second, we only explored the effect of metformin on the AMPK/eNOS pathway; future work should investigate other pathways activated by metformin administration. Third, noninvasive imaging technologies for rendering 3D images of the spinal cord vasculature, especially those that can be translated to the clinic, should be used in future studies.

Taken together, our findings show that functional recovery and blood vessel formation are decreased in aged mice compared with young mice post-SCI. Metformin played a neuroprotective role and enhanced neurological functional recovery after SCI in aged mice, possibly by promoting angiogenesis. Furthermore, the ability of metformin to promote angiogenesis and neurological functional recovery after SCI may be mediated by activation of the AMPK/eNOS pathway. Moreover, our study provides a novel therapeutic approach for promoting angiogenesis and functional recovery after SCI in aged mice.

Acknowledgments: *We would like to thank Prof. Hui Xie and other staff from the Movement System Injury and Repair Research Center, Xiangya Hospital, Central South University, Changsha, China; and Prof. Xiang-Hang Luo and other staff from the Department of Endocrinology, Endocrinology Research Center, Xiangya Hospital of Central South University, Changsha, China, for their kind assistance during the experiments.*

Author contributions: *Study design and supervision: CYD, JZH; experiment implementation: JYZ; data analysis: XLS, CJL, TQ, RDH, GYD; manuscript draft: JYZ, YC; manuscript revision: HBL, CYD, JZH. All authors contributed to and approved the final version of manuscript.*

Conflicts of interest: *The authors have no conflicts of interest relevant to this article.*

Availability of data and materials: *All data generated or analyzed during this study are included in this published article and its supplementary information files.*

Open peer reviewer: *Úrzula Franco-Enzástiga, University of Texas at Dallas, USA.*

Additional files:

Additional Figure 1: *Schematic of the experiment to explore the difference between young and aged mice.*

Additional Figure 2: *Schematic of the experiment to explore the effect of metformin treatment on aged SCI mice.*

Additional Figure 3: *Schematic of the experiment to explore the effect of Compound C on the aged SCI mice with metformin treatment.*

Additional Figure 4: *Aging exacerbates histological tissue repair at 14 days post-SCI.*

Additional Figure 5: *Identification of SCMECs.*

Additional Figure 6: *Compound C did not change the histology tissue architecture of spinal cord at 56 days post-SCI among different groups.*

Additional file 1: *Open peer review report 1.*

References

Alhowail A, Chigurupati S (2022) Research advances on how metformin improves memory impairment in "chemobrain". Neural Regen Res 17:15-19.

Ali DE, Shah M, Ali A, Malik MO, Rehman F, Badshah H, Ehtesham E, Vitale SG (2019) Treatment with metformin and combination of metformin plus pioglitazone on serum levels of IL-6 and IL-8 in polycystic ovary syndrome: a randomized clinical trial. Horm Metab Res 51:714-722.

Allen AR (1911) Surgery of experimental lesion of spinal cord equivalent to crush injury of fracture dislocation of spinal column: a preliminary report. J Am Med Assoc LVII:878-880.

Anisimov VN, Egormin PA, Piskunova TS, Popovich IG, Tyndyk ML, Yurova MN, Zabezhinski MA, Anikin IV, Karkach AS, Romanyukha AA (2010) Metformin extends life span of HER-2/neu transgenic mice and in combination with melatonin inhibits growth of transplantable tumors in vivo. Cell Cycle 9:188-197.

Arifin WN, Zahiruddin WM (2017) Sample size calculation in animal studies using resource equation approach. Malays J Med Sci 24:101-105.

Barzilai N, Crandall JP, Kritchevsky SB, Espeland MA (2016) Metformin as a tool to target aging. Cell Metab 23:1060-1065.

Basso DM, Fisher LC, Anderson AJ, Jakeman LB, McTigue DM, Popovich PG (2006) Basso Mouse Scale for locomotion detects differences in recovery after spinal cord injury in five common mouse strains. J Neurotrauma 23:635-659.

Benton RL, Maddie MA, Minnillo DR, Hagg T, Whittemore SR (2008) Griffonia simplicifolia isolectin B4 identifies a specific subpopulation of angiogenic blood vessels following contusive spinal cord injury in the adult mouse. J Comp Neurol 507:1031-1052.

Bharath LP, Agrawal M, McCambridge G, Nicholas DA, Hasturk H, Liu J, Jiang K, Liu R, Guo Z, Deeney J, Apovian CM, Snyder-Cappione J, Hawk GS, Fleeman RM, Pihl RMF, Thompson K, Belkina AC, Cui L, Proctor EA, Kern PA, et al. (2020) Metformin enhances autophagy and normalizes mitochondrial function to alleviate aging-associated inflammation. Cell Metab 32:44-55.e6.

Brigstock DR (2002) Regulation of angiogenesis and endothelial cell function by connective tissue growth factor (CTGF) and cysteine-rich 61 (CYR61). Angiogenesis 5:153-165.

Cabreiro F, Au C, Leung KY, Vergara-Irigaray N, Cochemé HM, Noori T, Weinkove D, Schuster E, Greene ND, Gems D (2013) Metformin retards aging in C. elegans by altering microbial folate and methionine metabolism. Cell 153:228-239.

Calvert JW, Gundewar S, Jha S, Greer JJ, Bestermann WH, Tian R, Lefer DJ (2008) Acute metformin therapy confers cardioprotection against myocardial infarction via AMPK-eNOS-mediated signaling. Diabetes 57:696-705.

Cao Y, Zhou Y, Ni S, Wu T, Li P, Liao S, Hu J, Lu H (2017) Three dimensional quantification of microarchitecture and vessel regeneration by synchrotron radiation microcomputed tomography in a rat model of spinal cord injury. J Neurotrauma 34:1187-1199.

Chaplan SR, Bach FW, Pogrel JW, Chung JM, Yaksh TL (1994) Quantitative assessment of tactile allodynia in the rat paw. J Neurosci Methods 53:55-63.

Chen D, Xia D, Pan Z, Xu D, Zhou Y, Wu Y, Cai N, Tang Q, Wang C, Yan M, Zhang JJ, Zhou K, Wang Q, Feng Y, Wang X, Xu H, Zhang X, Tian N (2016) Metformin protects against apoptosis and senescence in nucleus pulposus cells and ameliorates disc degeneration in vivo. Cell Death Dis 7:e2441.

Chen ZP, Mitchelhill KI, Michell BJ, Stapleton D, Rodriguez-Crespo I, Witters LA, Power DA, Ortiz de Montellano PR, Kemp BE (1999) AMP-activated protein kinase phosphorylation of endothelial NO synthase. FEBS Lett 443:285-289.

Devivo MJ (2012) Epidemiology of traumatic spinal cord injury: trends and future implications. Spinal Cord 50:365-372.

DiLoreto R, Murphy CT (2015) The cell biology of aging. Mol Biol Cell 26:4524-4531.

Donovan MJ, Lin MI, Wiegn P, Ringstedt T, Kraemer R, Hahn R, Wang S, Ibañez CF, Rafii S, Hempstead BL (2000) Brain derived neurotrophic factor is an endothelial cell survival factor required for intramyocardial vessel stabilization. Development 127:4531-4540.

Dumbrava DA, Surugiu R, Börger V, Ruscu M, Tertel T, Giebel B, Hermann DM, Popa-Wagner A (2022) Mesenchymal stromal cell-derived small extracellular vesicles promote neurological recovery and brain remodeling after distal middle cerebral artery occlusion in aged rats. Geroscience 44:293-310.

Duran CL, Borriello L, Karagiannis GS, Entenberg D, Oktay MH, Condeelis JS (2021) Targeting Tie2 in the tumor microenvironment: from angiogenesis to dissemination. Cancers (Basel) 13:5730.

Figley SA, Khosravi R, Legasto JM, Tseng YF, Fehlings MG (2014) Characterization of vascular disruption and blood-spinal cord barrier permeability following traumatic spinal cord injury. J Neurotrauma 31:541-552.

Graumann U, Ritz MF, Hausmann O (2011) Necessity for re-vascularization after spinal cord injury and the search for potential therapeutic options. Curr Neurovasc Res 8:334-341.

Hilton BJ, Bradke F (2017) Can injured adult CNS axons regenerate by recapitulating development? Development 144:3417-3429.

Hu J, Yang Z, Li X, Lu H (2016) C-C motif chemokine ligand 20 regulates neuroinflammation following spinal cord injury via Th17 cell recruitment. J Neuroinflammation 13:162.

Huang D, Wang FB, Guo M, Li S, Yan ML, Yu T, Wei M, Li JB (2015) Effect of combined treatment with rosuvastatin and protein kinase Cβ2 inhibitor on angiogenesis following myocardial infarction in diabetic rats. Int J Mol Med 35:829-838.

Ikeda Y, Aihara K, Yoshida S, Iwase T, Tajima S, Izawa-Ishizawa Y, Kihira Y, Ishizawa K, Tomita S, Tsuchiya K, Sata M, Akaike M, Kato S, Matsumoto T, Tamaki T (2012) Heparin cofactor II, a serine protease inhibitor, promotes angiogenesis via activation of the AMP-activated protein kinase-endothelial nitric-oxide synthase signaling pathway. J Biol Chem 287:34256-34263.

Isidori AM, Venneri MA, Fiore D (2016) Angiopoietin-1 and angiopoietin-2 in metabolic disorders: therapeutic strategies to restore the highs and lows of angiogenesis in diabetes. J Endocrinol Invest 39:1235-1246.

Joussen AM, Ricci F, Paris LP, Korn C, Quezada-Ruiz C, Zarbin M (2021) Angiopoietin/Tie2 signalling and its role in retinal and choroidal vascular diseases: a review of preclinical data. Eye (Lond) 35:1305-1316.

Kahn BB, Alquier T, Carling D, Hardie DG (2005) AMP-activated protein kinase: ancient energy gauge provides clues to modern understanding of metabolism. Cell Metab 1:15-25.

Kamarudin MNA, Sarker MMR, Zhou JR, Parhar I (2019) Metformin in colorectal cancer: molecular mechanism, preclinical and clinical aspects. J Exp Clin Cancer Res 38:491.

Kermani P, Hempstead B (2007) Brain-derived neurotrophic factor: a newly described mediator of angiogenesis. Trends Cardiovasc Med 17:140-143.

Kundi S, Bicknell R, Ahmed Z (2013) The role of angiogenic and wound-healing factors after spinal cord injury in mammals. Neurosci Res 76:1-9.

Lähteenvuo J, Rosenzweig A (2012) Effects of aging on angiogenesis. Circ Res 110:1252-1264.

Leech T, Chattipakorn N, Chattipakorn SC (2019) The beneficial roles of metformin on the brain with cerebral ischaemia/reperfusion injury. Pharmacol Res 146:104261.

Livak KJ, Schmittgen TD (2001) Analysis of relative gene expression data using real-time quantitative PCR and the 2(-Delta Delta C(T)) Method. Methods 25:402-408.

Long YC, Zierath JR (2006) AMP-activated protein kinase signaling in metabolic regulation. J Clin Invest 116:1776-1783.

Musi N, Hirshman MF, Nygren J, Svanfeldt M, Bavenholm P, Rooyackers O, Zhou G, Williamson JM, Ljunqvist O, Efendic S, Moller DE, Thorell A, Goodyear LJ (2002) Metformin increases AMP-activated protein kinase activity in skeletal muscle of subjects with type 2 diabetes. Diabetes 51:2074-2081.

Ng MT, Stammers AT, Kwon BK (2011) Vascular disruption and the role of angiogenic proteins after spinal cord injury. Transl Stroke Res 2:474-491.

Ni S, Cao Y, Jiang L, Luo Z, Lu H, Hu J, Wu T (2018) Synchrotron radiation imaging reveals the role of estrogen in promoting angiogenesis after acute spinal cord injury in rats. Spine (Phila Pa 1976) 43:1241-1249.

Ni S, Luo Z, Jiang L, Guo Z, Li P, Xu X, Cao Y, Duan C, Wu T, Li C, Lu H, Hu J (2019) UTX/KDM6A deletion promotes recovery of spinal cord injury by epigenetically regulating vascular regeneration. Mol Ther 27:2134-2146.

Pang P, Abbott M, Chang SL, Abdi M, Chauhan N, Mistri M, Ghofrani J, Fucci QA, Walker C, Leonardi C, Grady S, Halim A, Hoffman R, Lu T, Cao H, Tullius SG, Malek S, Kumar S, Steele G, Kibel A, et al. (2017) Human vascular progenitor cells derived from renal arteries are endothelial-like and assist in the repair of injured renal capillary networks. Kidney Int 91:129-143.

Paudel YN, Angelopoulou E, Piperi C, Shaikh MF, Othman I (2020) Emerging neuroprotective effect of metformin in Parkinson's disease: a molecular crosstalk. Pharmacol Res 152:104593.

Percie du Sert N, Hurst V, Ahluwalia A, Alam S, Avey MT, Baker M, Browne WJ, Clark A, Cuthill IC, Dirnagl U, Emerson M, Garner P, Holgate ST, Howells DW, Karp NA, Lazic SE, Lidster K, MacCallum CJ, Macleod M, Pearl EJ, et al. (2020) The ARRIVE guidelines 2.0: Updated guidelines for reporting animal research. PLoS Biol 18:e3000410.

Piskovatska V, Storey KB, Vaiserman AM, Lushchak O (2020) The use of metformin to increase the human healthspan. Adv Exp Med Biol 1260:319-332.

Pollak M (2017) The effects of metformin on gut microbiota and the immune system as research frontiers. Diabetologia 60:1662-1667.

Ren Y, Luo H (2021) Metformin: The next angiogenesis panacea? SAGE Open Med 9:20503121211001641.

Riggin CN, Weiss SN, Rodriguez AB, Raja H, Chen M, Schultz SM, Sehgal CM, Soslowsky LJ (2022) Increasing vascular response to injury improves tendon early healing outcome in aged rats. Ann Biomed Eng 50:587-600.

Ruck T, Bittner S, Epping L, Herrmann AM, Meuth SG (2014) Isolation of primary murine brain microvascular endothelial cells. J Vis Exp:e52204.

Samantaray S, Das A, Matzelle DC, Yu SP, Wei L, Varma A, Ray SK, Banik NL (2016) Administration of low dose estrogen attenuates persistent inflammation, promotes angiogenesis, and improves locomotor function following chronic spinal cord injury in rats. J Neurochem 137:604-617.

Sanz P, Serratosa JM, Sánchez MP (2021) Beneficial effects of metformin on the central nervous system, with a focus on epilepsy and Lafora disease. Int J Mol Sci 22:5351.

Sapieha P (2012) Eyeing central neurons in vascular growth and reparative angiogenesis. Blood 120:2182-2194.

Schlag MG, Hopf R, Redl H (2001) Serial recording of sensory, corticomotor, and brainstem-derived motor evoked potentials in the rat. Somatosens Mot Res 18:106-116.

Shi Z, Pan B, Feng S (2018) The emerging role of long non-coding RNA in spinal cord injury. J Cell Mol Med 22:2055-2061.

Shi Z, Zhou H, Lu L, Li X, Fu Z, Liu J, Kang Y, Wei Z, Pan B, Liu L, Kong X, Feng S (2017) The roles of microRNAs in spinal cord injury. Int J Neurosci 127:1104-1115.

Sinescu C, Popa F, Grigorean VT, Onose G, Sandu AM, Popescu M, Burnei G, Strambu V, Popa C (2010) Molecular basis of vascular events following spinal cord injury. J Med Life 3:254-261.

Singh A, Tetreault L, Kalsi-Ryan S, Nouri A, Fehlings MG (2014) Global prevalence and incidence of traumatic spinal cord injury. Clin Epidemiol 6:309-331.

Song WY, Ding H, Dunn T, Gao JL, Labastida JA, Schlagal C, Ning GZ, Feng SQ, Wu P (2021) Low-dose metformin treatment in the subacute phase improves the locomotor function of a mouse model of spinal cord injury. Neural Regen Res 16:2234-2242.

Takahashi N, Shibata R, Ouchi N, Sugimoto M, Murohara T, Komori K (2015) Metformin stimulates ischemia-induced revascularization through an eNOS dependent pathway in the ischemic hindlimb mice model. J Vasc Surg 61:489-496.

Tang Y, Wang L, Wang J, Lin X, Wang Y, Jin K, Yang GY (2016) Ischemia-induced angiogenesis is attenuated in aged rats. Aging Dis 7:326-335.

Tao T, Wu P, Wang Y, Liu W (2018) Comparison of glycemic control and β-cell function in new onset T2DM patients with PCOS of metformin and saxagliptin monotherapy or combination treatment. BMC Endocr Disord 18:14.

Tran AP, Warren PM, Silver J (2018) The biology of regeneration failure and success after spinal cord injury. Physiol Rev 98:881-917.

Ungvari Z, Tarantini S, Donato AJ, Galvan V, Csiszar A (2018) Mechanisms of Vascular Aging. Circ Res 123:849-867.

Ungvari Z, Valcarcel-Ares MN, Tarantini S, Yabluchanskiy A, Fülöp GA, Kiss T, Csiszar A (2017) Connective tissue growth factor (CTGF) in age-related vascular pathologies. Geroscience 39:491-498.

Vázquez-Manrique RP, Farina F, Cambon K, Dolores Sequedo M, Parker AJ, Millán JM, Weiss A, Déglon N, Neri C (2016) AMPK activation protects from neuronal dysfunction and vulnerability across nematode, cellular and mouse models of Huntington's disease. Hum Mol Genet 25:1043-1058.

Wang C, Liu C, Gao K, Zhao H, Zhou Z, Shen Z, Guo Y, Li Z, Yao T, Mei X (2016) Metformin preconditioning provide neuroprotection through enhancement of autophagy and suppression of inflammation and apoptosis after spinal cord injury. Biochem Biophys Res Commun 477:534-540.

Wang H, Zheng Z, Han W, Yuan Y, Li Y, Zhou K, Wang Q, Xie L, Xu K, Zhang H, Xu H, Wu Y, Xiao J (2020) Metformin promotes axon regeneration after spinal cord injury through inhibiting oxidative stress and stabilizing microtubule. Oxid Med Cell Longev 2020:9741369.

Wang Z, Chen Y, Chen X, Zheng X, Xu G, Yuan Z, Zhao H, Chen W, Li L, Zheng N, Shen X, Li Y, Qi X, Cai D (2019) The TrkB-T1 receptor mediates BDNF-induced migration of aged cardiac microvascular endothelial cells by recruiting Willin. Aging Cell 18:e12881.

Xu H, Chen K, Jia X, Tian Y, Dai Y, Li D, Xie J, Tao M, Mao Y (2015a) Metformin use is associated with better survival of breast cancer patients with diabetes: a meta-analysis. Oncologist 20:1236-1244.

Xu L, Wang S, Li B, Sun A, Zou Y, Ge J (2015b) A protective role of ciglitazone in ox-LDL-induced rat microvascular endothelial cells via modulating PPARγ-dependent AMPK/eNOS pathway. J Cell Mol Med 19:92-102.

Yu JW, Deng YP, Han X, Ren GF, Cai J, Jiang GJ (2016) Metformin improves the angiogenic functions of endothelial progenitor cells via activating AMPK/eNOS pathway in diabetic mice. Cardiovasc Diabetol 15:88.

Yuyun MF, Ng LL, Ng GA (2018) Endothelial dysfunction, endothelial nitric oxide bioavailability, tetrahydrobiopterin, and 5-methyltetrahydrofolate in cardiovascular disease. Where are we with therapy? Microvasc Res 119:7-12.

Zhang D, Tang Q, Zheng G, Wang C, Zhou Y, Wu Y, Xuan J, Tian N, Wang X, Wu Y, Xu H, Zhang X (2017a) Metformin ameliorates BSCB disruption by inhibiting neutrophil infiltration and MMP-9 expression but not direct TJ proteins expression regulation. J Cell Mol Med 21:3322-3336.

Zhang D, Xuan J, Zheng BB, Zhou YL, Lin Y, Wu YS, Zhou YF, Huang YX, Wang Q, Shen LY, Mao C, Wu Y, Wang XY, Tian NF, Xu HZ, Zhang XL (2017b) Metformin improves functional recovery after spinal cord injury via autophagy flux stimulation. Mol Neurobiol 54:3327-3341.

Zhang T, Wang F, Li K, Lv C, Gao K, Lv C (2020) Therapeutic effect of metformin on inflammation and apoptosis after spinal cord injury in rats through the Wnt/β-catenin signaling pathway. Neurosci Lett 739:135440.

Zhou G, Myers R, Li Y, Chen Y, Shen X, Fenyk-Melody J, Wu M, Ventre J, Doebber T, Fujii N, Musi N, Hirshman MF, Goodyear LJ, Moller DE (2001) Role of AMP-activated protein kinase in mechanism of metformin action. J Clin Invest 108:1167-1174.

P-Reviewer: Franco-Enzástiga Ú; C-Editor: Zhao M; S-Editors: Yu J, Li CH; L-Editors: Crow E, Yu J, Song LP; T-Editor: Jia Y

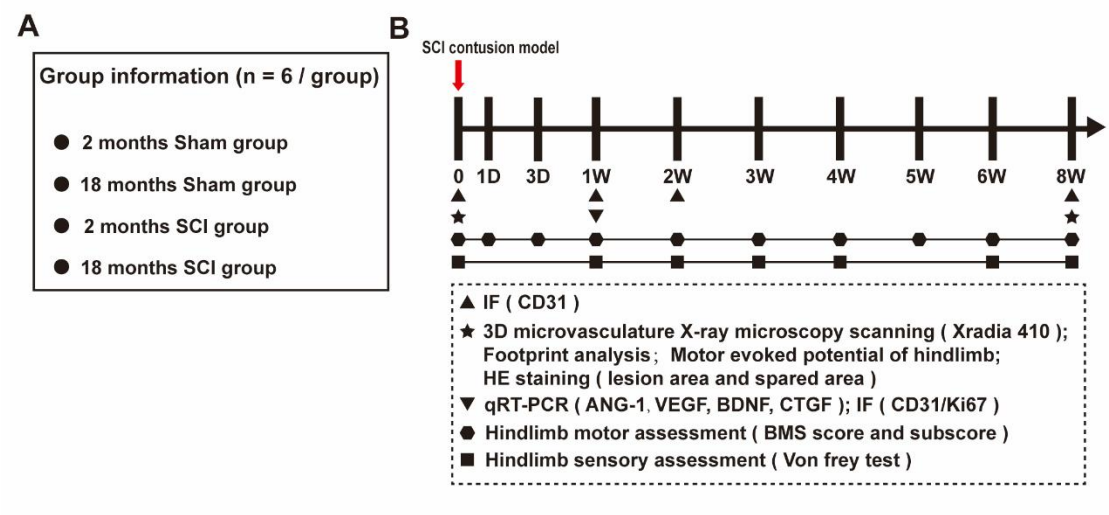

Additional Figure 1 Schematic of the experiment to explore the difference between young and aged mice.

ANG-1: Angiopoietin-1; *BDNF*: brain-derived neurotrophic factor; BMS: Basso Mouse Scale; *CTGF*: connective tissue growth factor; HE: hematoxylin-eosin; IF: immunofluorescence; SCI: spinal cord injury; *VEGF*: vascular endothelial growth factor.

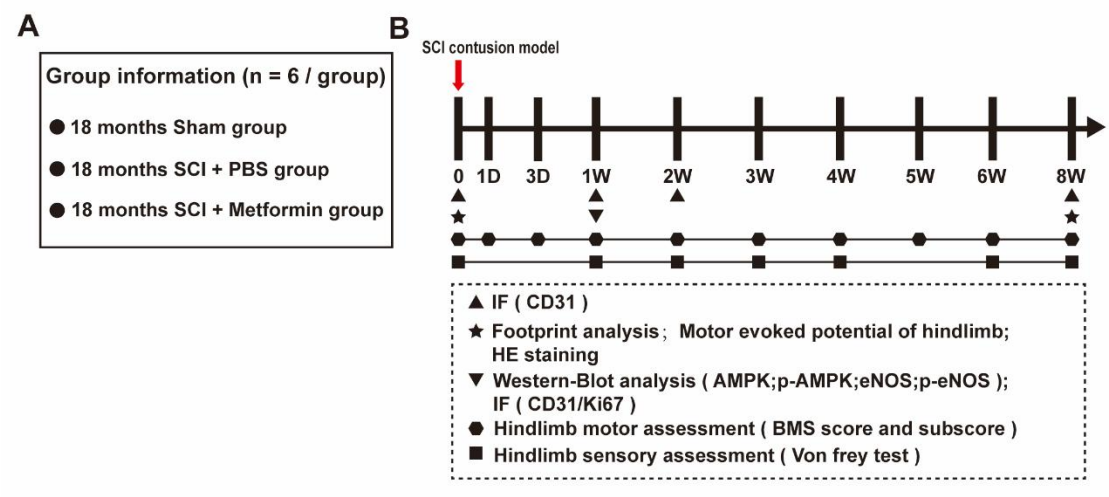

Additional Figure 2 Schematic of the experiment to explore the effect of metformin treatment on aged SCI mice.

AMPK: adenosine monophosphate-activated protein kinase; BMS: Basso Mouse Scale; HE: hematoxylin-eosin; IF: immunofluorescence; eNOS: endothelial nitric oxide synthase; p-AMPK: phosphor-AMPK; p-eNOS: phosphor-eNOS; PBS: phosphate buffer saline; SCI: spinal cord injury.

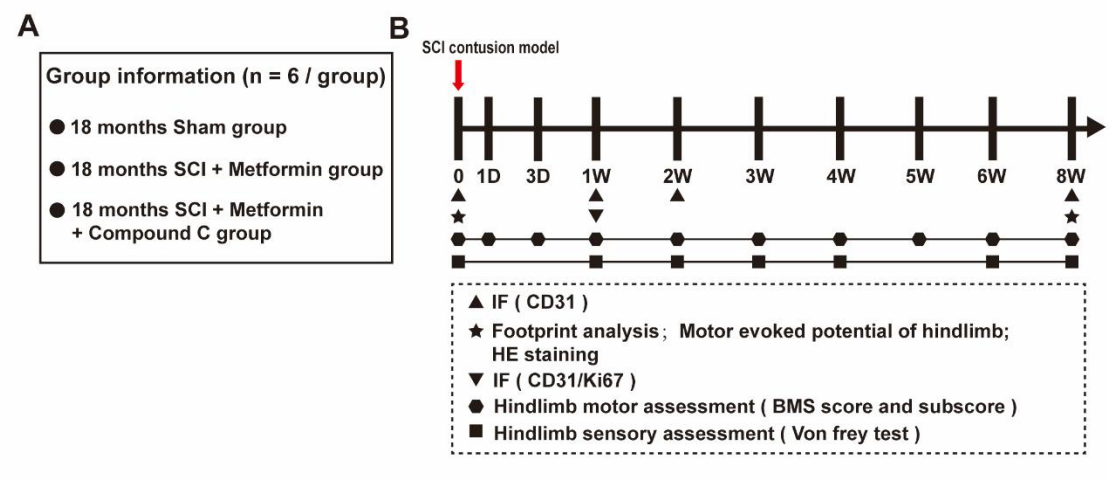

Additional Figure 3 Schematic of the experiment to explore the effect of Compound C on the aged SCI mice with metformin treatment.

BMS: Basso Mouse Scale; Compound C: an adenosine monophosphate-activated protein kinase inhibitor; HE: hematoxylin-eosin; IF: immunofluorescence; SCI: Spinal cord injury.

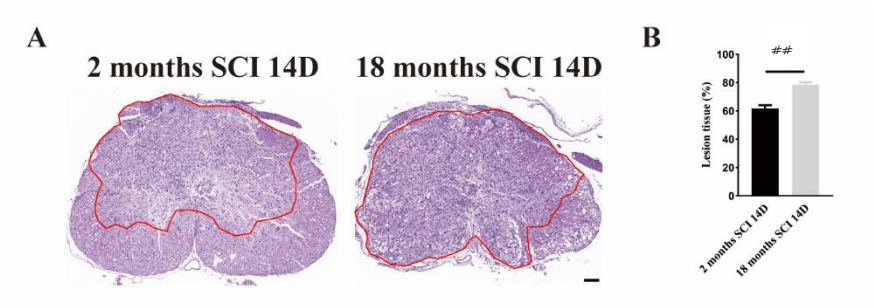

Additional Figure 4 Aging exacerbates histological tissue repair at 14 days post-SCI.

(A) The representative transverse sections at 500 μm rostrally from the injured epicenter with hematoxylin-eosin staining in aged and young mice at 14 days post-SCI. The aged mice presented more severe pathological change compared with young mice. Red lines indicate the lesion area. Scale bar: 200 μm. (B) Quantification of lesion area in A. The data are presented as the mean ± SEM (n = 6 per group). ##P < 0.01 (two-tailed Student's t-test). SCI: Spinal cord injury.

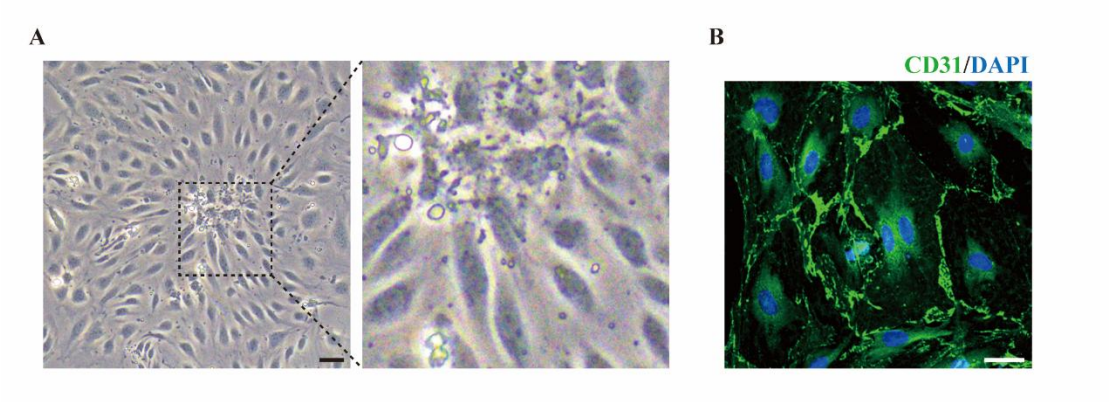

Additional Figure 5 Identification of SCMECs.

(A) The morphology of SCMECs. (B) Representative immunofluorescence image of SCMECs (CD31-green-Alexa Fluor® 488). Scale bars: 20 μm. DAPI: 4',6-Diamidino-2-phenylindole; SCMECs: spinal cord microvascular endothelial cells.

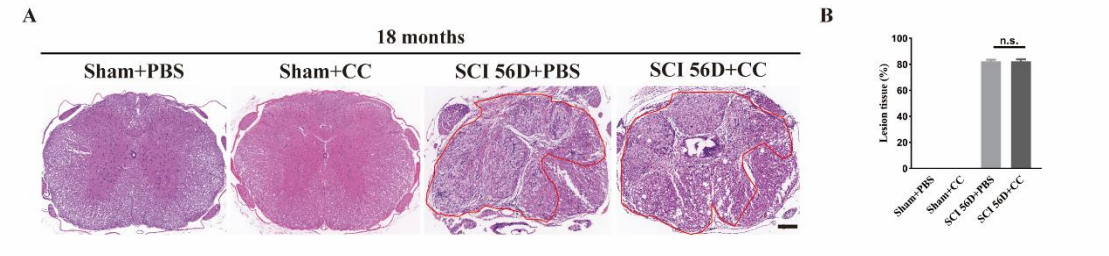

Additional Figure 6 Compound C did not change the histology tissue architecture of spinal cord at 56 days post-SCI among different groups.

(A) The representative transverse sections at the injury epicenter with hematoxylin-eosin staining in aged mice after administration with Compound C or PBS before injury and post-56 dpi. Compound C didn't change the tissue architecture of spinal cord before and after SCI. Red lines indicate the lesion area. Scale bar: 200 μm. (B) Quantification of lesion area in A. The data are presented as the mean ± SEM (n = 6 per group), and were analyzed by two-tailed Student's t-test. CC: Compound C, an AMPK inhibitor; n.s.: no significance; PBS: phosphate buffer saline; SCI: spinal cord injury.